Mapping of Enzyme Kinetics on a Microfluidic Device

Hoon Suk Rho[1], Alexander Thomas Hanke[2], Marcel Ottens[2], Han Gardeniers[1]*

1 Mesoscale Chemical Systems Group, MESA+ Institute for Nanotechnology, University of Twente, Enschede, The Netherlands, **2** BioProcess Engineering group, Department of Biotechnology, Faculty of Applied Sciences, Delft University of Technology, Delft, The Netherlands

* j.g.e.gardeniers@utwente.nl

Abstract

A microfluidic platform or "microfluidic mapper" is demonstrated, which in a single experiment performs 36 parallel biochemical reactions with 36 different combinations of two reagents in stepwise concentration gradients. The volume used in each individual reaction was 36 nl. With the microfluidic mapper, we obtained a 3D enzyme reaction plot of horseradish peroxidase (HRP) with Amplex Red (AR) and hydrogen peroxide (H_2O_2), for concentration ranges of 11.7 μM to 100.0 μM and 11.1 μM to 66.7 μM for AR and H_2O_2, respectively. This system and methodology could be used as a fast analytical tool to evaluate various chemical and biochemical reactions especially where two or more reagents interact with each other. The generation of dual concentration gradients in the present format has many advantages such as parallelization of reactions in a nanoliter-scale volume and the real-time monitoring of processes leading to quick concentration gradients. The microfluidic mapper could be applied to various problems in analytical chemistry such as revealing of binding kinetics, and optimization of reaction kinetics.

Introduction

Enzymes, biological catalysts, play important roles in various biological processes such as food fermentation, bio-analysis, protein synthesis, and drug discovery [1,2]. Enzymes can be characterized by their catalytic effect on reaction kinetics [3]. The essential information to understand the mechanism of enzyme-catalyzed reactions is the rate of reaction accelerated by the enzyme under different conditions. However, in most industrial and pharmaceutical applications, the rate of the enzymatic reactions are not only dependent on one major parameter but also two or more factors that interact with each other and strongly influence the behavior of the target system [4]. For example, apoenzymes require a cofactor, cosubstrate, or coenzyme to be functionalized as holoenzymes to catalyze the conversion of a substrate [2,5]. Hence the dynamic interactions between various effective parameters according to their concentrations has important implications on the characterization and optimization of enzyme systems, or more generally of reaction networks in the fields of Systems Biology [6].

Practically, to create a single three dimensional (3D) response plot [7,8], dual concentration gradients of two different reagents are required. Nevertheless, generating dual concentration gradients is almost impracticable with conventional test tubes and pipettes because only one test condition can be manually handled at a given time. Microtiter plate readers coupled with robotic fluid delivery systems can provide accurate gradient profiles and also dual concentration gradients of two reagents to obtain a 3D response. However, the long experimentation time and elaborate handling of reagents that are required for these methods hamper the observation in quantitative and amalgamative behaviors of target molecules. Furthermore, the involved high sample consumption is challenging because large volume causes very high cost in the early discovery phases of enzymes and substrates.

With a strong demand to generate the desired combinations of mixtures in an extremely small volumes, several microfluidic devices have been developed by adapting networking of continuous flows [9–18], parallel reactors [19–22], and micro-droplets [23–26]. These miniaturized devices have shown many clear advantages by applying concentration gradients on a chip. These include the requirement of low sample consumption and also the integration of sample preparation steps such as metering, mixing, incubation, and optical detection. Flow-based microfluidic systems provide a flexible linear gradient and also fast changing of the gradient profile which is beneficial for the study of cell biology, for example, cell culture [13,14] and chemotaxis [16–18]. However, the continuous tracing of an event in an individual reaction, which is critical to determine the rate of reaction, remains challenging for kinetic studies. The devices made by multilayer soft lithography are especially efficient in performing multiple reactions with the large scale integration of reactors [19–21,27–31]. With these devices the incubation of target mixtures in a closed system without fluid flow allowed both continuous monitoring and long term observation of the reactions. Although the previous devices performed multiple reactions with a series of concentrations of a single reagent, rapid generation of dual concentration gradients of different reagents is a desirable advancement, helpful in achieving a bird's-eye view on a complicated enzyme system and in revealing the reaction network and interaction of factors in a certain target system.

Here, we developed an integrated system that can create dual reagent concentration gradients on a microfluidic chip, which allows the subsequent construction of 3D response plots from the generated concentration gradients. The device has 36 parallel reactors to conduct 36 individual enzyme reactions with concentration gradients of two substrates at a constant concentration of an enzyme. Using the system, we performed 36 horseradish peroxidase (HRP) catalyzed reactions with dual gradients of Amplex Red (AR) and hydrogen peroxide (H_2O_2). With a single experiment we obtained a 3D kinetic plot that contains all the detailed information for understanding the kinetics of the target enzyme system.

Materials and Methods

Chip design

The microfluidic mapper consists of 36 parallel reactors as shown in Fig 1 (Photolithographic mask design is shown in S1 Fig). The fluidic channels were filled with food colored dyes to visualize the microchannel layout of the device. Fig 1A shows the connections of channels for loading four reagents, enzyme (orange color), substrate I (yellow color), substrate II (blue color), and buffer (green color) solutions. The mixing ratio of four reagents in a reactor is determined by the length of the channels. The final combinations and compositions of the reagents in the 36 reactors are summarized in Table 1. Fig 1B shows the process flow in a reactor. During loading reagents into the device, the reactor is separated into four loading sites for four reagents by closing metering valves. After loading, the metering valves are open while side valves are closed
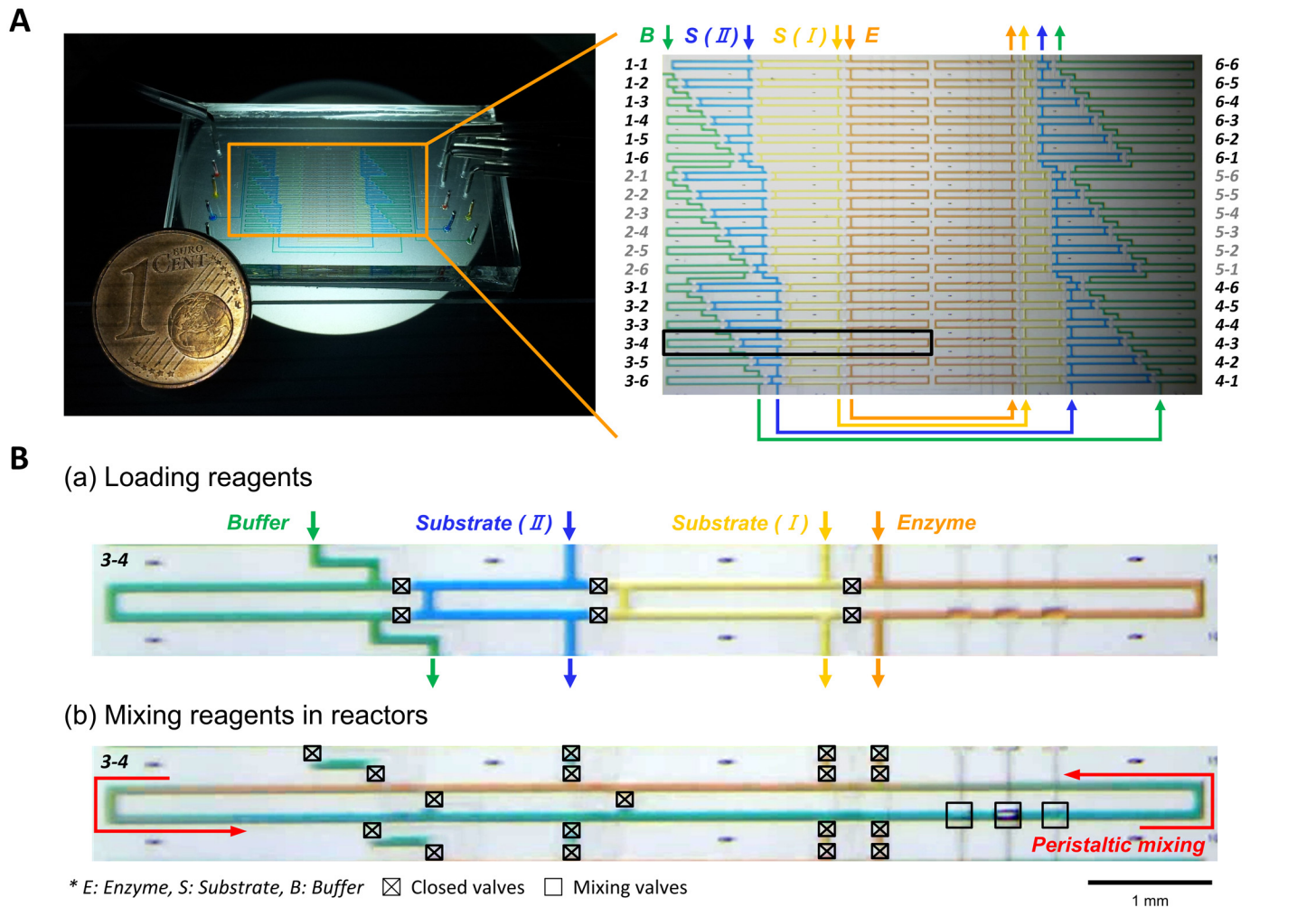
Fig 1. Design and operation of complete microfluidic device. (A) Photo of the device in connections with control ports (left) and 36 parallel reactors with food colored dyes loaded. (B) Operation of a single reactor element in the device. Metering valves were closed when the reagent solutions were loaded (a) and side valves were closed for the formation of a loop-shaped reactor (b). The solutions in the reactor were mixed by operating mixing valves in a sequence.

to form a single loop-shaped reactor. Then the mixing valves are actuated in a specific sequence, (100), (110), (010), (011), (001), (101), where 0 is open and 1 is closed, to generate fluid flow for active mixing of the reagents (S1 Movie).

Chip fabrication

The device consists of two polydimethylsiloxane (PDMS) layers, a fluidic layer and a control layer, and was fabricated by multilayer soft lithography [32,33]. Masks were designed by Cle-Win software (WieWeb software, Hengelo, The Netherlands) and printed on 5" soda lime glasses by LBPG Heidelberg DWL200 (Heidelberg Instruments Mikrotechnik GmbH, Germany). Positive photoresist (AZ 40 XT, MicroChemicals GmbH, Ulm, Germany) was spun onto 4" silicon wafers. The wafers were exposed to UV light through masks and developed. The mold for the fluidic layer was reflowed by heating at 140°C for one minute. The fluidic layer was made by pouring uncured PDMS (GE RTV615, elastomer:cross-linker = 7:1) onto the mold. The control layer was produced by spin-coating uncured PDMS (elastomer:cross-linker = 20:1) onto the master mold at 2300 rpm for one minute. The fluidic layer was cured

Table 1. Combinations and compositions of reagents in 36 parallel reactors to accommodate dual concentration gradients of two substrates.

Reactor number	Channel length* [µm]				Volume [nl]				Final concentration		
	Enzyme	Substrate #1	Substrate #2	Buffer	Enzyme	Substrate #1	Substrate #2	Buffer	Enzyme (E_0: initial Con.)	Substrate #1 ($S1_0$: initial Con.)	Substrate #2 ($S2_0$: initial Con.)
1–1	6000	6000	6000	0	12	12	12	0	$0.333\,E_0$	$0.333\,S1_0$	$0.333\,S2_0$
1–2	6000	6000	5000	1000	12	12	10	2	$0.333\,E_0$	$0.333\,S1_0$	$0.278\,S2_0$
1–3	6000	6000	4000	2000	12	12	8	4	$0.333\,E_0$	$0.333\,S1_0$	$0.222\,S2_0$
1–4	6000	6000	3000	3000	12	12	6	6	$0.333\,E_0$	$0.333\,S1_0$	$0.167\,S2_0$
1–5	6000	6000	2000	4000	12	12	4	8	$0.333\,E_0$	$0.333\,S1_0$	$0.111\,S2_0$
1–6	6000	6000	1000	5000	12	12	2	10	$0.333\,E_0$	$0.333\,S1_0$	$0.056\,S2_0$
2–1	6000	5000	6000	1000	12	10	12	2	$0.333\,E_0$	$0.278\,S1_0$	$0.333\,S2_0$
2–2	6000	6000	5000	2000	12	10	10	4	$0.333\,E_0$	$0.278\,S1_0$	$0.278\,S2_0$
2–3	6000	6000	4000	3000	12	10	8	6	$0.333\,E_0$	$0.278\,S1_0$	$0.222\,S2_0$
2–4	6000	6000	3000	4000	12	10	6	8	$0.333\,E_0$	$0.278\,S1_0$	$0.167\,S2_0$
2–5	6000	6000	2000	5000	12	10	4	10	$0.333\,E_0$	$0.278\,S1_0$	$0.111\,S2_0$
2–6	6000	6000	1000	6000	12	10	2	12	$0.333\,E_0$	$0.278\,S1_0$	$0.056\,S2_0$
3–1	6000	4000	6000	2000	12	8	12	4	$0.333\,E_0$	$0.222\,S1_0$	$0.333\,S2_0$
3–2	6000	6000	5000	3000	12	8	10	6	$0.333\,E_0$	$0.222\,S1_0$	$0.278\,S2_0$
3–3	6000	6000	4000	4000	12	8	8	8	$0.333\,E_0$	$0.222\,S1_0$	$0.222\,S2_0$
3–4	6000	6000	3000	5000	12	8	6	10	$0.333\,E_0$	$0.222\,S1_0$	$0.167\,S2_0$
3–5	6000	6000	2000	6000	12	8	4	12	$0.333\,E_0$	$0.222\,S1_0$	$0.111\,S2_0$
3–6	6000	6000	1000	7000	12	8	2	14	$0.333\,E_0$	$0.222\,S1_0$	$0.056\,S2_0$
4–1	6000	3000	6000	3000	12	6	12	6	$0.333\,E_0$	$0.167\,S1_0$	$0.333\,S2_0$
4–2	6000	6000	5000	4000	12	6	10	8	$0.333\,E_0$	$0.167\,S1_0$	$0.278\,S2_0$
4–3	6000	6000	4000	5000	12	6	8	10	$0.333\,E_0$	$0.167\,S1_0$	$0.222\,S2_0$
4–4	6000	3000	3000	6000	12	6	6	12	$0.333\,E_0$	$0.167\,S1_0$	$0.167\,S2_0$
4–5	6000	6000	2000	7000	12	6	4	14	$0.333\,E_0$	$0.167\,S1_0$	$0.111\,S2_0$
4–6	6000	6000	1000	8000	12	6	2	16	$0.333\,E_0$	$0.167\,S1_0$	$0.056\,S2_0$
5–1	6000	3000	6000	4000	12	4	12	8	$0.333\,E_0$	$0.111\,S1_0$	$0.333\,S2_0$
5–2	6000	6000	5000	5000	12	4	10	10	$0.333\,E_0$	$0.111\,S1_0$	$0.278\,S2_0$
5–3	6000	6000	4000	6000	12	4	8	12	$0.333\,E_0$	$0.111\,S1_0$	$0.222\,S2_0$
5–4	6000	3000	3000	7000	12	4	6	14	$0.333\,E_0$	$0.111\,S1_0$	$0.167\,S2_0$
5–5	6000	6000	2000	8000	12	4	4	16	$0.333\,E_0$	$0.111\,S1_0$	$0.111\,S2_0$
5–6	6000	6000	1000	9000	12	4	2	18	$0.333\,E_0$	$0.111\,S1_0$	$0.056\,S2_0$
6–1	6000	3000	6000	5000	12	2	12	10	$0.333\,E_0$	$0.056\,S1_0$	$0.333\,S2_0$
6–2	6000	6000	5000	6000	12	2	10	12	$0.333\,E_0$	$0.056\,S1_0$	$0.278\,S2_0$
6–3	6000	6000	4000	7000	12	2	8	14	$0.333\,E_0$	$0.056\,S1_0$	$0.222\,S2_0$
6–4	6000	3000	3000	8000	12	2	6	16	$0.333\,E_0$	$0.056\,S1_0$	$0.167\,S2_0$
6–5	6000	6000	2000	9000	12	2	4	18	$0.333\,E_0$	$0.056\,S1_0$	$0.111\,S2_0$
6–6	6000	6000	1000	10000	12	2	2	20	$0.333\,E_0$	$0.056\,S1_0$	$0.056\,S2_0$

* Channel width: 100 µm, channel height: 19.8 ± 0.3 µm (measured before reflowing process, n = 10)

for 45 minutes at 80°C and peeled off from the mold. After punching holes for inlets and outlets with a 25-gauge punch (Syneo Co., Angleton, TX, USA) the fluidic layer was aligned over the control layer. The aligned layers were baked for 1 hour at 80°C, after which the layers were peeled off from the mold and holes for the connections with control ports were punched. The PDMS device was placed on a pre-cleaned glass slide (Fisher Scientific, Landsmeer, The

Netherlands) and baked in the oven at 80°C for 12 hours to advance adhesion. To prevent non-specific binding of biomolecules, fluidic channels were treated with copolymer pluronic 10 g/L (Millipore, Zug, Switzerland) for 5 minutes before use and washed with reaction buffer solution for 30 minutes.

Chip operation

The microfluidic device was controlled by a pneumatic control system. Micro-valves were operated by applying compressed nitrogen gas into control channels. The pneumatic control system was automated by combining pressure regulators, 3/2-way solenoid valves, and Easy-Port USB digital I/O controller (all from Festo, Festo BV, The Netherlands). The system was automatically controlled by a custom-built LabVIEW (National Instruments Co.) program.

Data processing

We used a stereo microscope (Motic SMZ168, Lab Agency Benelux BV, The Netherlands) equipped with a CMOS camera (Moticam 3.0) for recording peristaltic mixing phenomena in the device. We used an inverted fluorescent microscope (Leica DMI 5000M, 10X and 20X Objectives, Leica Microsystems BV, The Netherlands) equipped with an automatic XY-stage (Oasis PCI XY control unit), and a digital camera (Leica DFC300 FX, Leica Microsystems BV, The Netherlands) for acquisition of time-lapse images to monitor fluorescent intensities in each of the 36 reactors. Time interval between two acquired fluorescent images of neighboring reactors was 3 seconds and between two time-lapse images of the same reactor was 100 seconds (S2 Fig). All the acquired images were processed and analyzed by the time series analyzer of Image J software (http://rsb.info.nih.gov/ij/). Kinetic data were analyzed using a nonlinear regression analysis program (Enzyme Kinetic Module, SigmaPlot, Systat Software, Inc.).

Chip validation

100 μM of fluorescein (Sigma-Aldrich Chemie BV, Zwijndrecht, The Netherlands) solution was prepared in Milli-Q water (Millipore Co.). The fluorescein solution was loaded into one loading site of the 36 reactors while the other three loading sites were filled with Milli-Q water. After mixing the solutions in the reactors for 1 minute, the fluorescent images of the 36 reactors were acquired by a Leica I3 filter cube (excitation: BP 450–490 nm; emission: LP 515 nm).

Enzyme reaction

100 μM of resorufin (Sigma-Aldrich Chemie BV, Zwijndrecht, The Netherlands) solution was prepared in Milli-Q water for the generation of a standard curve. Amplex Red Hydrogen Per-oxide/Peroxidase Assay Kit was obtained from Invitrogen (Invitrogen, Fisher Scientific, Land-smeer, The Netherlands). Stock solutions of 100 U/mL of HRP and 2 mM of AR were prepared in reaction buffer (0.25 M sodium phosphate, pH 7.4) and stored at -20°C. The stock solutions were diluted with reaction buffer immediately before use. 30% of hydrogen peroxide solution was obtained from Sigma-Aldrich (Zwijndrecht, The Netherlands) and diluted with Milli-Q water before use. The fluorescent signal from resorufin was observed by a Leica N 2.1 filter cube (excitation: BP 515–560 nm; emission: LP 590 nm). For the off-chip measurement of the resorufin fluorescent signal we used a spectrometer (Maya 200 Pro, Ocean Optics BV, Duiven, The Netherlands) with a xenon light source (HPX-2000, Ocean Optics BV, Duiven, The Netherlands) and a cuvette (fluorescence cell, 105.251-QS, Hellma BV, Nieuwegein, The Netherlands).

Results and Discussion

Device calibration (peristaltic mixing and metering)

Enhanced mixing and accurate metering are the most important capabilities of the device for the study of kinetics with parallel reactors. To validate and calibrate the device we tested the efficiency of our peristaltic mixing system and the accuracy in the generation of concentration gradient on the device. For the study of the mixing performance of the device we introduced red food dye solution into the loading site for an enzyme and Milli-Q water into the substrate I, substrate II, and buffer loading sites (Fig 2A). The three mixing valves were operated by cycling through the following six states (1 0 0), (1 1 0), (0 1 0), (0 1 1), (0 0 1), and (1 0 1), in sequence to achieve peristaltic mixing of the solutions in a reactor. The operating frequencies varied
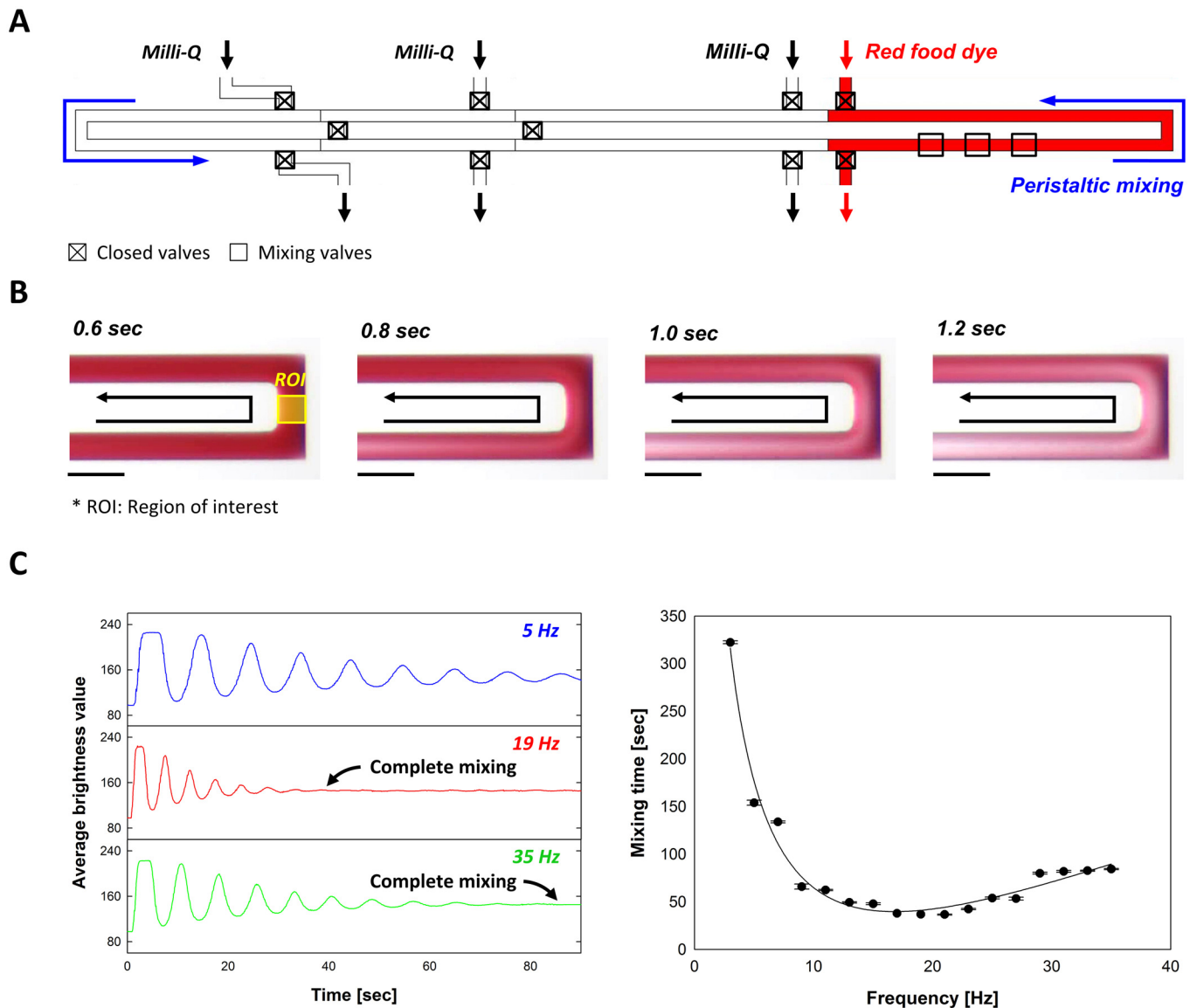

Fig 2. Peristaltic mixing on the device. (A) Composition of solutions for the study of mixing efficiency of the device, (B) Time-lapse microscope images of mixing of two liquid phases (200 μm scale bars are shown), and (C) Time series analysis of the change of average brightness value in a micro-mixer and relationship between the operating frequencies and complete mixing time.

doi:10.1371/journal.pone.0153437.g002

from 1 Hz to 35 Hz. Fig 2B shows time-lapse microscope images of mixing red dye solution and water. The circulation motion of the fluids was monitored and a time series analysis of the change of the average brightness values was performed at the ROI (region of interest, in Fig 2B) by Image J software. By operating the mixing valves in a sequence, Poiseuille flow was generated and the parabolic profile of the flow was stretched in the channel. The stretched interface between two liquid phases caused fast diffusion of the molecules. The mixing speed is dependent on the operating frequency of the valves. Fig 2C (left) shows the change of average brightness value at the ROI over time for various cycling frequencies. Corresponding to the degree of mixing, the fluctuation of the average brightness value steadily decreased until the average brightness reached a constant value. The complete mixing time, when the two solutions started to distribute uniformly, was evaluated to determine the mixing efficiency. Fig 2C (right) shows the relationship between the pumping frequencies and the complete mixing time. The mixing time is exponentially decreased with the increase of the frequency of the operating cycles below the cutoff frequency, 19 Hz [34]. The maximum operating frequency is approximately 35 Hz and matches with the limitation of the response time of the solenoid valves.

To demonstrate and validate the metering functionality of the device, we formed the concentration gradient of fluorescein and obtained fluorescence intensities in 36 reactors. Fig 3A shows the design of the compositions of reagents in the reactors. Each reactor has four loading sites for enzyme (orange), substrate I (yellow), substrate II (blue), and buffer (green) and the volumes of the reagents in the reactor are determined by the lengths of channels. As a negative
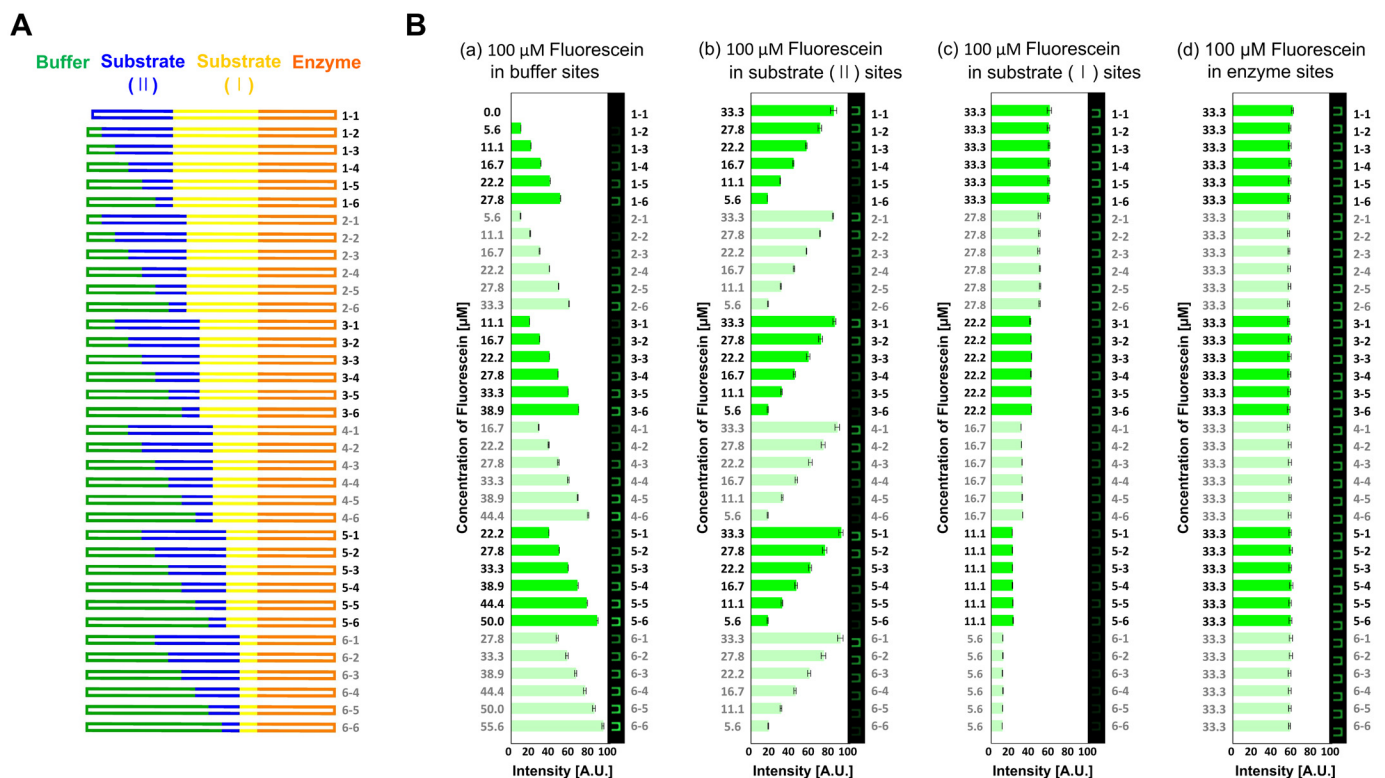
Fig 3. Generation of concentration gradient of fluorescein. (A) Design of the compositions of solutions in 36 reactors. Each reactor consists of four loading sites for enzyme (orange), substrate I (yellow), substrate II (blue), and buffer (green). (B) Fluorescence intensities of 36 reactors with concentration gradients of fluorescein as a negative control. The gradient of concentration of fluorescein was obtained by loading fluorescein solution into only one loading site while Milli-Q water was introduced into the other three sites. The obtained fluorescence intensities measured in the 36 reactors match with the target compositions (error bars represent the standard deviation from three measurements).

doi:10.1371/journal.pone.0153437.g003

control to validate the capability of the device on metering reagents we transferred 100 μM of fluorescein and Milli-Q water into the device. We filled one of the four loading sites with fluorescein solution and the remaining sites with Milli-Q water. Then we mixed the solutions for 1 minute by peristaltic mixing and obtained the fluorescent intensities of 36 reactors. Fig 3B shows the obtained fluorescent intensities of 36 reactors when only one loading site—(a) buffer, (b) substrate II, (c) substrate I, and (d) enzyme site—was filled with fluorescein solution and the other three sites were filled with Milli-Q. We performed each measurement three times and error bars in the graphs represent the standard deviation of the mean. The different fluorescent intensities correlated to the different metering ratios of the reagents in the reactors show accurate agreement with the target compositions of the reagents.
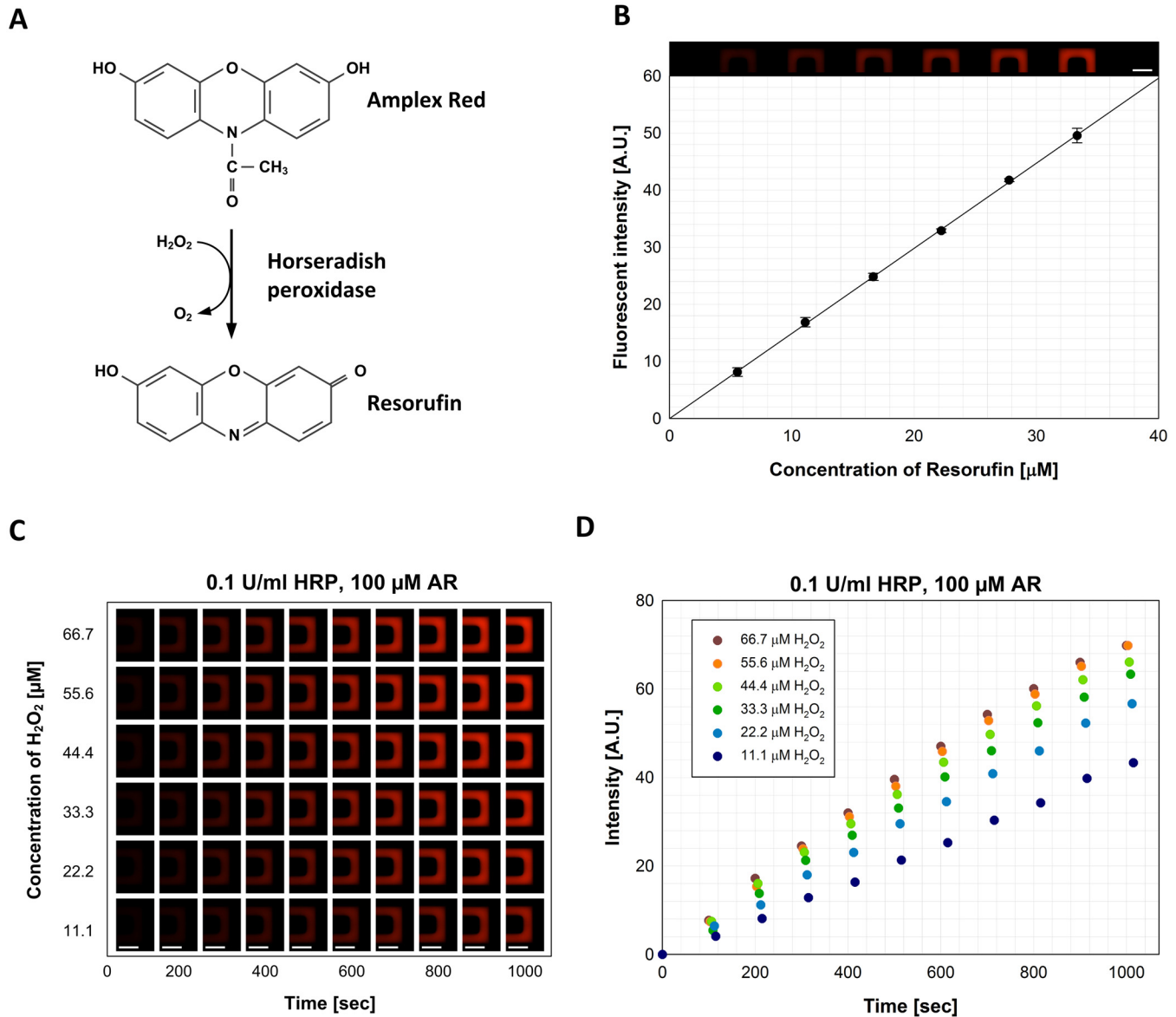
Parallel enzymatic reactions on a chip

To demonstrate the feasibility of the device for a study of enzyme kinetics, we performed 36 parallel HRP-catalyzed reactions with a series of concentration changes of AR and H_2O_2. HRP oxidizes nonfluorescent AR to a highly fluorescent product, resorufin, by employing H_2O_2 as a cosubstrate (Fig 4A). [35] The kinetic properties of an enzyme are determined by the rate of reaction as a function of the concentrations of a substrate (S1 File). [2,3,36] Hence monitoring the resorufin yield oxidized by HRP according to the concentrations of two substrates, AR and H_2O_2, provides detailed information to understand the catalytic behavior of HRP as well as the attributions of the substrates in the reactions. Fig 4B shows a standard curve to quantify the concentration of resorufin according to its fluorescent intensity in the reactor for tracing the product formation in the reaction. The concentration gradient of resorufin ranging from 5.6 μM to 33.3 μM with an increment of 5.6 μM was obtained in the device by introducing 100 μM of resorufin into an enzyme loading site and reaction buffer into substrate I, substrate II, and buffer loading sites. The acquired fluorescent images show the different concentrations of resorufin in 6 reactors and the standard curve shows the fluorescent intensity according to the increase in the concentration of resorufin.

To determine the kinetic parameters, we measured the rates of 36 HRP-catalyzed reactions according to various concentrations of AR and H_2O_2 by filling the enzyme site with 0.3 U/ml of HRP, the substrate I site with 300 μM of AR, the substrate II site with 200 μM of H_2O_2, and buffer site with reaction buffer. Due to the pre-designed different metered volumes of reagents in each processor, the final concentration of HRP was 0.1 U/ml, and the final concentrations of AR and H_2O_2 were varied from 16.7 μM to 100.0 μM with an increment of 16.7 μM and ranged from 11.1 μM to 66.7 μM with an increment of 11.1 μM, respectively (S1 Table). After mixing the reagents time-lapse fluorescent images of the reactors were acquired for the kinetic traces. The time courses of the product yield in 6 reactors from 1–1 to 1–6 are shown in Fig 4C and 4D (additional data for all 36 reactors in S3 Fig). The increase in the fluorescent intensity was attributed to the formation of fluorescent product, resorufin. Since the concentrations of HRP and AR are constant, the different rates of reactions are only influenced by the H_2O_2 concentration in the 6 reactors.

The initial rates of the reactions for 10 minutes after mixing were fitted with the Michaelis-Menten equation and kinetic parameters, K_m and V_{max}, were determined by using a nonlinear regression analysis program, Sigmaplot Enzyme Kinetics Module. Fig 5A shows the rates of HRP-catalyzed reactions with dual concentration gradients of AR and H_2O_2 in a 3D plot, where x-axis, y-axis, and z-axis represent the AR concentration, the H_2O_2 concentration, and the rate of reaction, respectively. With the 3D plot detailed information about the influences of AR and H_2O_2 on the kinetics was obtained by plot projections on the xz and yz planes. Fig 5B shows the xz projection of the 3D plot. Based on a single Michaelis-Menten plot in the

Fig 4. Parallel enzyme reactions on a chip. (**A**) Amplex Red, a nonfluorescent substrate, produces a highly fluorescent product, resorufin, in response to H_2O_2 upon the oxidation by HRP. (**B**) The relationship between the concentration of resorufin and its fluorescent intensity. The fluorescent images show the different concentrations of resorufin in reactors and the standard curve shows the change of fluorescent intensity with a response to the concentration of resorufin (200 µm scale bars are shown). (**C**) Time-lapse fluorescent images show resorufin formation in 6 reactors (reactor 1–1 to 1–6). (**D**) The increase in fluorescent intensity in the different reactors according to growing resorufin yield during enzymatic reactions of HRP with a constant concentration of AR and various concentrations of H_2O_2.

projection that shows the change of the reaction rate according to the concentration of AR at a specific concentration of H_2O_2, the kinetic parameters, K_m and V_{max}, were calculated (S2 Table). In the same manner we determined K_m and V_{max} at 6 different concentrations of H_2O_2 and the relationship between K_m (or V_{max}) and the H_2O_2 concentration was plotted in Fig 5D. The Michaelis-Menten plots obtained by the yz projection of the 3D plot and K_m and V_{max} determined by the Michaelis-Menten plots are shown in Fig 5C and 5E. We performed off-chip HRP-catalyzed reactions with a volume of 100 µl at various concentrations of H_2O_2, 2.5 µM, 5 µM, 10 µM, 15 µM, and 20 µM, and a constant concentration of AR, 50 µM (the
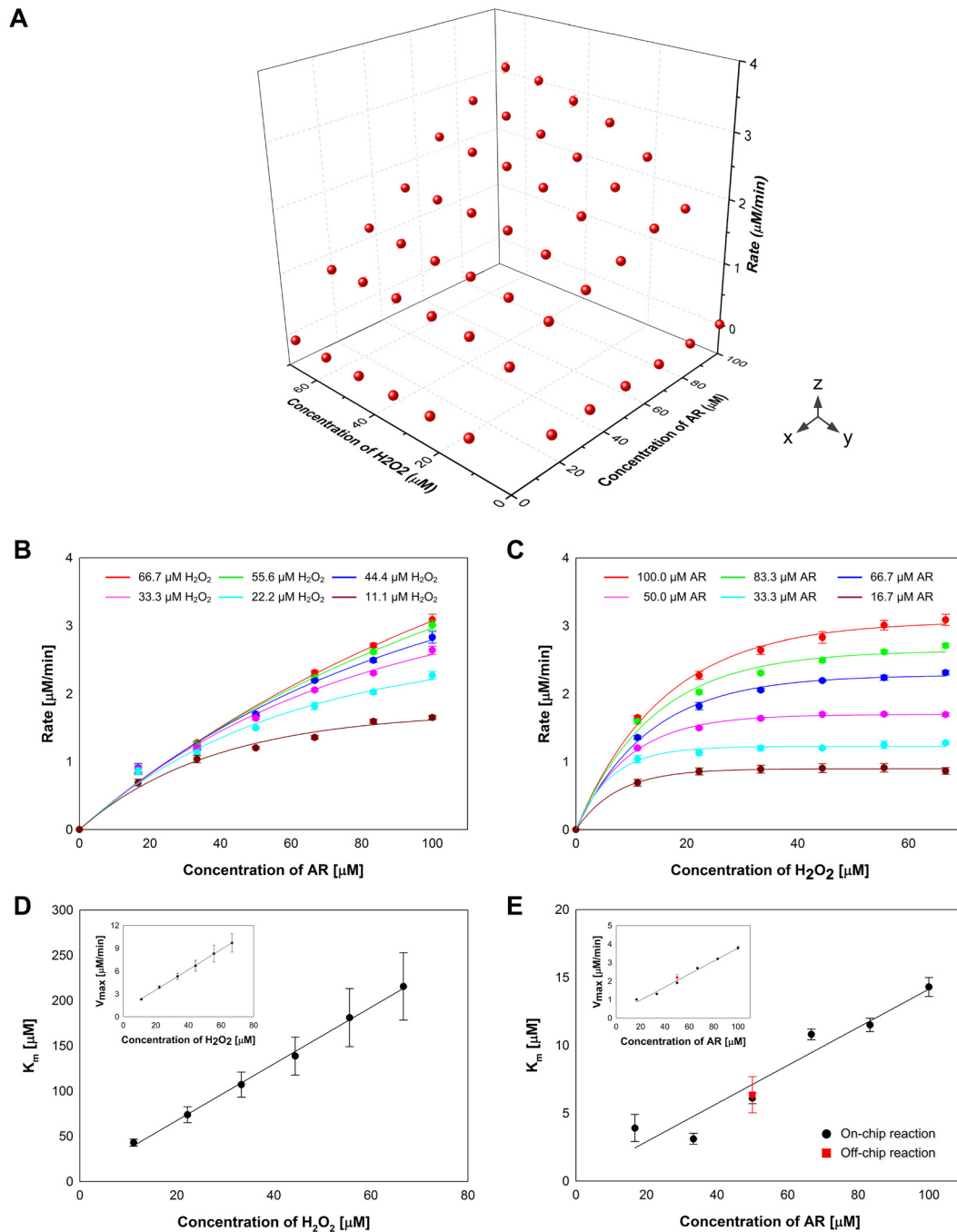
Fig 5. Michaelis-Menten plots of the enzymatic reaction of HRP with AR and H$_2$O$_2$. The initial rates of the HRP-catalyzed reactions with various concentrations of two substrates are plotted in 3D **(A)**. Based on xz projection **(B)** and yz projection **(C)** of the 3D plot, K$_m$ and V$_{max}$ values are calculated and plotted in **(D)** and **(E)**. The K$_m$ and V$_{max}$ values from off-chip reactions are shown in (E).

doi:10.1371/journal.pone.0153437.g005

detailed information is provided in S4 Fig). The values of K$_m$ and V$_{max}$ obtained from the off-chip experiments were 6.4 ± 1.3 and 2.2 ± 0.2, respectively (Fig 5E). Comparing with the values of K$_m$ and V$_{max}$ from the on-chip reactions, 6.1 ± 0.4 and 1.9 ± 0.0, the deviation was 5.3% for K$_m$ and 13.7% for V$_{max}$.

Conclusions

Dual-gradient analysis and 3D reaction plots have been used by researchers for the fast evaluation of reaction characteristics [20,37,38]. Using microtiter-plates and pipettes, the dual-gradient methodology can produce a single 3D plot instead of two 2D plots. A wider spread of the concept in chemistry and biology has been limited mainly by issues of time, man power and material consumption. And despite the fact that 3D reaction profiling and 3D binding kinetics have been reported for proteomics and genomics, there are but a few tools to show 3D data profiling from a single experiment. Automated microfluidics, which works with nanoliter-scale reagents, can fulfil the need for such tools. For that to become possible, flexible protocols for the creation of concentration gradients in microfluidic devices is desired, because each application demands a different concentration range and a different number of reagents [21,22,39]. Commonly, flexibility can be achieved by adopting a modular approach, which is used frequently in engineering design. With our new device approach, we have achieved the desired flexibility in concentration gradient generation by using parallel mixer-reactor architectures. Based on the concentration of reagents loaded into the reactors, different concentrations can be achieved in an automated way, by controlled mixing and dilution. The device also includes different loading sites in each reactor to generate the concentrations of positive and negative controls for the characterization of reactions, in a single experiment. In addition, by using time-wise tracing of kinetic reactions and plotting them as a 3D landscape plot, characterization of kinetic reactions is possible with the resulting determination of kinetic parameters, such as K_m and V_{max} even for multiple substrate systems. This is one of the novel features of the present device. This flexibility in fast characterization of reactions could be expanded for various kinetic assays such as enzymatic kinetics, binding kinetics, and drug discovery.

The 3D reaction plot from a single experiment is useful for the fast evaluation of enzyme-catalyzed reactions. 3D plots could be constructed for single enzyme and two substrates system, single substrate with enzyme and coenzyme system, or single enzyme and single substrate with different pH [2,3]. If the final goal of the kinetic experiments is to evaluate the performance of reagents, then the rigor of mathematical analysis to determine kinetic parameters could be avoided, as rapid evaluation could be possible from the direct observation of 3D plot.

Supporting Information

S1 Fig. Photolithographic mask design (Clewin software) of a microfluidic mapper.
(TIF)

S2 Fig. Image acquisition of 36 reactors. Time interval between two acquisitions of the fluorescent images of neighboring reactors (ΔT) was 3 seconds and between two time-lapse images of the same reactor ($T_{n+1} - T_n$) was 100 seconds for the kinetic study in this work.(A) The moving direction of an automatic stage for scanning 36 reactors, and (B) An example of two time-lapse image acquisitions and plotting of the intensity according to time for 6 reactors.
(TIF)

S3 Fig. Time-lapse fluorescent images and time courses of HRP reactions. (A) Reactor 1–1 to 1–6, (B) Reactor 2–1 to 2–6, (C) Reactor 3–1 to 3–6, (D) Reactor 4–1 to 4–6, (E) Reactor 5–1 to 5–6, and (F) Reactor 6–1 to 6–6 (200 μm scale bars are shown).
(TIF)

S4 Fig. Off-chip HRP-catalyzed reactions. (A) Standard curve to quantify the concentration of resorufin according to its fluorescence intensity for tracing the product formation in the HRP-catalyzed reaction. The fluorescence intensity of resorufin was measured at various

concentrations of resorufin ranged from 10 μM to 60 μM with an increment of 10 μM (n = 3). (B) The change of fluorescence intensity of resorufin according to resorufin yield during HRP reactions. The increases in the resorufin fluorescence intensities were monitored at various concentrations of H_2O_2 (0.1 U/ml of HRP and 50 μM of AR). (C) Michaelis-Menten plot of the reactions. The initial rates of the reactions for 10 minutes were fitted with the Michaelis-Menten equation and kinetic parameters were calculated by Sigmaplot Enzyme Kinetic Module. The obtained K_m and V_{max} were 6.4 ± 1.3 and 2.2 ± 0.2, respectively (n = 3) Comparing with the values of K_m and V_{max} from the on-chip reactions, 6.1 ± 0.4 and 1.9 ± 0.0, the deviation was 5.3% for K_m and 13.7% for V_{max}.
(TIF)

S1 File. Michaelis-Menten equation.
(PDF)

S1 Movie. Operation of a microfluidic mapper.
(AVI)

S1 Table. Combinations and compositions of reagents for HRP reactions with AR and H_2O_2.
(PDF)

S2 Table. Michaelis-Menten reaction parameters for AR and H_2O_2 in the various conditions.
(PDF)

Acknowledgments

Author Contributions

Conceived and designed the experiments: HSR ATH HG. Performed the experiments: HSR. Analyzed the data: HSR ATH HG. Contributed reagents/materials/analysis tools: HSR. Wrote the paper: HSR ATH MO HG.

References

1. Nelson DL, Lehninger AL, Cox MM (2008) Lehninger principles of biochemistry: Macmillan.

2. Shuler ML, Kargi F (2002) Bioprocess engineering: Prentice Hall New York.

3. Segel IH (1975) Enzyme kinetics: Wiley, New York.

4. Harvey D (2000) Modern analytical chemistry: McGraw-Hill New York.

5. Price NC, Frey PA (2001) Fundamentals of enzymology. Biochemistry and Molecular Biology Education 29: 34–35.

6. Kitano H (2002) Systems biology: a brief overview. Science 295: 1662–1664. PMID: 11872829

7. Sammon JW (1969) A nonlinear mapping for data structure analysis. IEEE Transactions on computers: 401–409.

8. Arnold VI (1989) Mathematical methods of classical mechanics: Springer Science & Business Media.

9. Hadd AG, Raymond DE, Halliwell JW, Jacobson SC, Ramsey JM (1997) Microchip device for performing enzyme assays. Analytical Chemistry 69: 3407–3412. PMID: 9286159

10. Dertinger SK, Chiu DT, Jeon NL, Whitesides GM (2001) Generation of gradients having complex shapes using microfluidic networks. Analytical Chemistry 73: 1240–1246.

11. Seong GH, Heo J, Crooks RM (2003) Measurement of enzyme kinetics using a continuous-flow micro-fluidic system. Analytical chemistry 75: 3161–3167. PMID: 12964765

12. Neils C, Tyree Z, Finlayson B, Folch A (2004) Combinatorial mixing of microfluidic streams. Lab on a Chip 4: 342–350. PMID: 15269802

13. Chung BG, Flanagan LA, Rhee SW, Schwartz PH, Lee AP, Monuki ES, et al. (2005) Human neural stem cell growth and differentiation in a gradient-generating microfluidic device. Lab on a Chip 5: 401–406. PMID: 15791337

14. Paliwal S, Iglesias PA, Campbell K, Hilioti Z, Groisman A, Levchenko A (2007) MAPK-mediated bimodal gene expression and adaptive gradient sensing in yeast. Nature 446: 46–51. PMID: 17310144

15. Frank T, Tay S (2013) Flow-switching allows independently programmable, extremely stable, high-throughput diffusion-based gradients. Lab on a Chip 13: 1273–1281. doi: 10.1039/c3lc41076e PMID: 23386049

16. Mehling M, Frank T, Albayrak C, Tay S (2015) Real-time tracking, retrieval and gene expression analysis of migrating human T cells. Lab on a Chip 15: 1276–1283. doi: 10.1039/c4lc01038h PMID: 25512266

17. Jeon NL, Baskaran H, Dertinger SK, Whitesides GM, Van De Water L, Toner M (2002) Neutrophil chemotaxis in linear and complex gradients of interleukin-8 formed in a microfabricated device. Nature biotechnology 20: 826–830. PMID: 12091913

18. Saadi W, Wang S-J, Lin F, Jeon NL (2006) A parallel-gradient microfluidic chamber for quantitative analysis of breast cancer cell chemotaxis. Biomedical microdevices 8: 109–118. PMID: 16688570

19. Hong JW, Studer V, Hang G, Anderson WF, Quake SR (2004) A nanoliter-scale nucleic acid processor with parallel architecture. Nature biotechnology 22: 435–439. PMID: 15024389

20. Maerkl SJ, Quake SR (2007) A systems approach to measuring the binding energy landscapes of transcription factors. Science 315: 233–237. PMID: 17218526

21. Jambovane S, Duin EC, Kim S-K, Hong JW (2009) Determination of Kinetic Parameters, K M and k cat, with a Single Experiment on a Chip. Analytical chemistry 81: 3239–3245. doi: 10.1021/ac8020938 PMID: 19338287

22. Wang J, Sui G, Mocharla VP, Lin RJ, Phelps ME, Kolb HC, et al. (2006) Integrated microfluidics for parallel screening of an in situ click chemistry library. Angew Chem Int Ed Engl 45: 5276–5281. PMID: 16927322

23. Song H, Tice JD, Ismagilov RF (2003) A microfluidic system for controlling reaction networks in time. Angew Chem Int Ed Engl 42: 768–772. PMID: 12596195

24. Bui M-PN, Li CA, Han KN, Choo J, Lee EK, Seong GH (2011) Enzyme kinetic measurements using a droplet-based microfluidic system with a concentration gradient. Analytical chemistry 83: 1603–1608. doi: 10.1021/ac102472a PMID: 21280615

25. Jambovane S, Kim DJ, Duin EC, Kim S-K, Hong JW (2011) Creation of stepwise concentration gradient in picoliter droplets for parallel reactions of matrix metalloproteinase II and IX. Analytical chemistry 83: 3358–3364. doi: 10.1021/ac103217p PMID: 21456571

26. Miller OJ, El Harrak A, Mangeat T, Baret J-C, Frenz L, El Debs B, et al. (2012) High-resolution dose–response screening using droplet-based microfluidics. Proceedings of the National Academy of Sciences 109: 378–383.

27. Melin J, Quake SR (2007) Microfluidic large-scale integration: the evolution of design rules for biological automation. Annu Rev Biophys Biomol Struct 36: 213–231. PMID: 17269901

28. Dai J, Yoon SH, Sim HY, Yang YS, Oh TK, Kim JF, et al. (2013) Charting microbial phenotypes in multiplex nanoliter batch bioreactors. Analytical chemistry 85: 5892–5899. doi: 10.1021/ac400648z PMID: 23581968

29. Yang Y, Swennenhuis JF, Rho HS, Le Gac S, Terstappen LW (2014) Parallel single cancer cell whole genome amplification using button-valve assisted mixing in nanoliter chambers. PLoS ONE 9: e107958. doi: 10.1371/journal.pone.0107958 PMID: 25233459

30. Gardeniers JGE, Rho HS, Ottens M, Hanke AT (2015) Microfluidic device and method for batch adsorption. European patent application.

31. Yang Y, Rho HS, Stevens M, Tibbe AG, Terstappen L (2015) Microfluidic device for DNA amplification of single cancer cells isolated from whole blood by self-seeding microwells. Lab Chip.

32. Xia Y, Whitesides GM (1998) Soft lithography. Annual review of materials science 28: 153–184.

33. Unger MA, Chou H-P, Thorsen T, Scherer A, Quake SR (2000) Monolithic microfabricated valves and pumps by multilayer soft lithography. Science 288: 113–116. PMID: 10753110

34. Goulpeau J, Trouchet D, Ajdari A, Tabeling P (2005) Experimental study and modeling of polydimethylsiloxane peristaltic micropumps. Journal of Applied Physics 98: 044914.

35. Zhou M, Diwu Z, Panchuk-Voloshina N, Haugland RP (1997) A stable nonfluorescent derivative of resorufin for the fluorometric determination of trace hydrogen peroxide: applications in detecting the activity of phagocyte NADPH oxidase and other oxidases. Analytical biochemistry 253: 162–168. PMID: 9367498

36. Lineweaver H, Burk D (1934) The determination of enzyme dissociation constants. Journal of the American Chemical Society 56: 658–666.

37. Fraga CG, Bruckner CA, Synovec RE (2001) Increasing the number of analyzable peaks in comprehensive two-dimensional separations through chemometrics. Analytical chemistry 73: 675–683. PMID: 11217781

38. Khajeh M, Botana A, Bernstein MA, Nilsson M, Morris GA (2010) Reaction kinetics studied using diffusion-ordered spectroscopy and multiway chemometrics. Analytical chemistry 82: 2102–2108. doi: 10.1021/ac100110m PMID: 20131871

39. Hamon M, Jambovane S, Bradley L, Khademhosseini A, Hong JW (2013) Cell-based dose responses from open-well microchambers. Analytical chemistry 85: 5249–5254. doi: 10.1021/ac400743w PMID: 23570236